



A calibrated weakest-link model for probabilistic assessment of LCF life considering notch size effects

Xi Liu^a, Rongqiao Wang^{a,b}, Dianyin Hu^{a,b,c,*}, Jianxing Mao^{a,c}



^a School of Energy and Power Engineering, Beihang University, Beijing 100191, China
^b Beijing Key Laboratory of Aero-Engine Structure and Strength, Beijing 100191, China
^c Research Institute of Aero-engine, Beihang University, Beijing 100191, China

ARTICLE INFO

Keywords:
 Size effect
 Weakest-link method
 Low cycle fatigue
 Probabilistic life prediction
 Bayesian inference method

ABSTRACT

This study proposes a calibrated weakest-link model for probabilistic life in low cycle fatigue (LCF) regime considering the geometric size effect and the statistical size effect. Weakest-link model is first extended to LCF regime by using damage parameter, and then calibrated based on crack propagation process. Meanwhile, experiments on standard smooth specimens and central hole plate (CHP) specimens are conducted. To improve model accuracy, parameters in the proposed model are calibrated by using Bayesian inference method. Finally, probabilistic LCF life is predicted for CHP specimens with different scales, which shows good agreement with test data.

1. Introduction

Aeroengine's turbine disk often made of nickel-based superalloys is subjected to cyclic loads at service, which generally causes it to fail by low cycle fatigue (LCF) at notch locations such as bolt holes. The notch fatigue limit is different from the strength based on the tests with smooth specimens loaded under the maximum stress at the notch root, due to the notch size effects induced by the stress gradient and size difference [1], which are defined as geometric size effect and statistical size effect, respectively [2]. The geometric size effect exists for the notched specimen with stress concentration, while the statistical size effect represents the difference in fatigue life for the specimens with different volumes. Therefore, in order to ensure the prediction accuracy of fatigue crack initiation and propagation life for actual components, it is necessary to quantify these two kinds of notch size effects.

Non-local method has been developed to quantify the notch size effects on the fatigue crack initiation life, in which the theory of critical distance (TCD) [3–9] method and the weakest-link method [10–13] are two principal approaches. The TCD method adapts well for the component's fatigue life evaluation when considering the geometric size effect since it chooses the effective stress/stain at the critical distance [14–16]. However, several studies have proved that TCD method brings in a large error in describing the statistical size effect [1,17,18], because the effect of microstructure cannot be considered in this method. In contrast, the weakest-link method is a microscopic model based on the probabilistic approach [19]. It describes the size effects through

statistical modelling the size and spatial distribution of the microstructure. For instance, the weakest-link method widely uses Weibull statistics model to predict the probabilistic fatigue life [20], which assumes uniform size distribution and spatial Poisson distribution, expressed as

$$P_f = 1 - \exp \left[- \left(\frac{\bar{\sigma}}{\sigma_0} \right)^{b_\sigma} \right]; \quad \bar{\sigma} = \left(\frac{1}{V_0} \int_V (\sigma - \sigma_{th})^{b_\sigma} dV \right)^{1/b_\sigma} \quad (1)$$

where, P_f is the cumulative failure probability of a solid with volume V suffering from stress σ ; $\bar{\sigma}$ is effective stress, V_0 is reference volume; σ_0 , σ_{th} and b_σ are material parameters. In Eq.(1), the effective stress is utilized to quantify geometric size effect as well as statistical size effect, which is calculated by integrating the stress σ in each unit volume dV [21,22].

The weakest-link method was originally used for estimating fatigue limit and fatigue life in high cycle fatigue (HCF) regime for brittle [10,23] or quasi-brittle [24–26] materials. Recently, a few studies have focused on extending weakest-link method to the LCF regime. Based on the weakest-link theory, Zhu *et al.* [27] presented a mechanical-probabilistic modeling of size effect in LCF regime by using experimental data for different geometrical smooth specimens. This study employed Basquin equation to describe fatigue life which is effective in high-cycle low-strain fatigue regime [28] while incapable of describing plastic behavior in LCF failure. To this end, Li *et al.* [29] established the relationship between damage parameter and fatigue life in replace of

* Corresponding author at: School of Energy and Power Engineering, Beihang University, Beijing 100191, China.
 E-mail address: hdy@buaa.edu.cn (D. Hu).

Nomenclature	
a	crack length
a_f	final crack length
$a_{f,1}$	final crack length of specimen 1
$a_{f,2}$	final crack length of specimen 2
a_i	initial crack length
b_σ	shape parameter in Weibull's weakest-link model
b_N	Weibull shape parameter
C	constant in SWT model
d	grain size
dV	unit volume
D_0	diameter of standard specimen
E	tolerance
k	material parameter in SWT model
k_g, k'	material parameter in Tomkins model
K	multiplier
$L(\cdot)$	likelihood distribution
m	Weibull shape parameter
n	number of specimens
N_e	experimental fatigue life (cycles)
N_f	fatigue life (cycles)
N_p	predicted fatigue life (cycles)
N_0	initial fatigue life (cycles)
N_0	Weibull scale parameter
N_1	fatigue life of specimen 1
N_2	fatigue life of specimen 2
$N(V)$	number of microcracks within V
P_f	failure probability
P_{f1}	failure probability of specimen 1
P_{f2}	failure probability of specimen 2
$p(V_0)$	failure probability of each microcell unit
R_e	strain ratio
R_σ	stress ratio
S_{-1}	fatigue limit
T	temperature
V	volume
V_1	volume of specimen 1
V_2	volume of specimen 2
V_0	reference volume
V_E	effective volume
V_{E1}	effective volume of specimen 1
V_{E2}	effective volume of specimen 2
V_i	volume of i -th unit
w	damage parameter
\bar{w}	effective damage parameter
w_{SWT}	SWT parameter
w_{th}	threshold of damage parameter
w_0	normalized damage parameter
w_i	damage parameter of i -th unit
σ	equivalent stress
$\bar{\sigma}$	effective stress
σ_0	scale parameter in Weibull's weakest-link method
σ_{th}	threshold stress
σ_e	effective stress
σ_e	standard deviation of fitting error
δw_0	material parameter in SWT model
ΔN	life dispersion band
$\Delta \sigma$	applied stress range
$\Delta \varepsilon_t$	total strain range
τ	material parameter in Tomkins model
γ	natural logarithm of the ratio of the final crack length and initial crack length
ε	strain
ε_r	fitting error
<i>Superscripts</i>	
\min	minimum value within an element
\max	maximum value within an element
<i>Subscripts</i>	
i	i -th element
<i>Abbreviations</i>	
CHP	central hole plate
FE	finite element
HCF	high cycle fatigue
LCF	low cycle fatigue
NS	nominal stress
MCMC	Markov Chain Monte Carlo
TCD	theory of critical distance

Basquin model during the derivation of weakest-link model, which is proved to be more reasonable for LCF life estimation. Inspired by this, we employed the weakest-link model in LCF failure as proposed in Ref. [29] by combining the microscopic physical mechanism of weakest-link method, and then verified the rationality of the damage parameter used in LCF regime.

In traditional weakest-link method, the influence of statistical size effect on fatigue life is treated as a negative one, namely, the increase in specimen size will reduce fatigue strength and fatigue life [17,21,30,31]. However, the positive size effect has been found during the crack propagation because the critical crack length increases with a larger size/volume. Since the crack propagation life for ductile steels accounts for a large proportion in the total fatigue life compared to the crack initiation life [32,33], it is necessary to consider the size effect in the crack propagation stage. Like what Blason found, he demonstrated the characterization of the twofold size effects by analyzing HCF test results for the specimens with the same shape but different size, and further extended the fatigue property from standard specimens to large components [34]. After building the probabilistic relationship between crack propagation rate and fatigue life, Zhu *et al* [27] explained the statistical size effect for crack propagation using finite element (FE)

simulation. However, a probabilistic fatigue life model to fully describe both geometric size effect and statistical size effect during crack initiation and propagation stage is lacking. Therefore, in order to describe the notch size effects effectively, the weakest-link method needs to be developed during the crack propagation.

On the other hand, considering that the weakest-link model is highly sensitive to Weibull parameters [13,29], it is necessary to accurately estimate the parameters toward improving the reliability of components. But there are usually limited or even unavailable test data for aero-engine's components [35]. Thus, Bayesian inference method is introduced in this work to calibrate Weibull parameters, since it has been widely used for model calibration due to its splendid behavior in processing small samples [36–41].

In this regard, this study first explores the influence of the notch size effects during the crack initiation and crack propagation based on the LCF tests on standard specimens and CHP specimens. Then, the weakest-link method is extended to LCF regime by introducing the damage parameter, and further calibrated based on the statistical size effect during the crack propagation. By using the calibrated weakest-link model, probabilistic LCF life prediction for the CHP specimen is conducted, during which process Bayesian inference method is applied

to calibrate the model parameters in order to improve the prediction accuracy. Moreover, the discussion and conclusions are provided.

2. LCF tests

2.1. Material and specimens

LCF tests were carried out on standard specimens and CHP specimens, in which standard specimens were referred to ASTM standard E606 [42], while CHP specimens with four different sizes but similar shape were designed coincident with the stress distribution of the actual turbine disk as shown in Fig. 1. The dimensions and stress concentration factors K_t for each kind of CHP specimen are listed in Table 1. All of the specimens are made of GH4169 superalloy (a kind of nickel-based superalloy in China which is similar to Inconel 718), with crystal phase shown in Fig. 2.

2.2. LCF tests data

Strain-controlled LCF tests were conducted on standard specimens at $R_e = 0.1$ and $T = 600^\circ\text{C}$. The results are shown in Fig. 3.

To explore the geometric size effect, LCF tests were conducted on 100%-scale CHP specimens at $R_\sigma = 0.1$ and $T = 600^\circ\text{C}$, as shown in Fig. 4(a). In comparison, LCF tests of CHP specimens with 80%-60%-and 40%-scales were conducted under constant nominal stress (NS) to study the effect of statistical size effect, as shown in Fig. 4(b).

2.3. Test results analysis

2.3.1. Distribution of grain size

The grain size of GH4169 specimen is gathered using the image processing software Image-Pro Plus, and then processed using statistical method to obtain the distribution. From the histogram graph of grain size plotted in Fig. 5, it is shown the grain size varies from 5 μm to 9.5 μm . Then the probability distribution of grain size is established based on the statistical results in Fig. 5, as follows

$$f(\ln d) = 0.3323 \exp \left[-\left(\frac{\ln d - 1.943}{0.4724} \right)^2 \right] \quad (2)$$

in which d represents grain size, $\ln d$ is natural logarithm of the grain size.

2.3.2. LCF life model based on damage parameter

During LCF analysis, the relationship between damage parameter w and fatigue life N_f is established using a three-parameter power function model [29]. By introducing the SWT parameter w_{SWT} [43], the relationship is expressed as

$$w^k \cdot N_f = C \quad (3)$$

$$w = w_{\text{SWT}} - \delta w_0 = \Delta \varepsilon_t \sigma^{\max} \quad (4)$$

in which $\Delta \varepsilon_t$ and σ^{\max} are total strain range and maximum stress respectively. C , k , δw_0 are material parameters, which are fitted using the test results of standard specimens, as listed in Table 2. The predicted fatigue life is compared with the experimental data, as shown in Fig. 6. By using the life dispersion band ΔN to describe the predicted error in Eq. (5), the ΔN is within 1.6.

$$\Delta N = \max \left\{ \frac{N_p}{N_e} (N_p > N_e), \frac{N_e}{N_p} (N_p \leq N_e) \right\} \quad (5)$$

2.3.3. Fatigue crack growth model

After the tests, the fracture surface morphology of the standard and CHP specimens is observed as shown in Fig. 7. Both cracks are initiated from one single source at the surface of the specimens. The crack

propagation accounts for a large part of the cross section [30], and obviously, the fatigue life is mainly dominated by the crack propagation life.

To describe the crack propagation feature, Tomkins model [44] is used to model fatigue crack in the LCF regime. For LCF tests under constant stress amplitude, the crack growth rate is expressed as

$$\frac{da}{dN} = \frac{\Delta \sigma^\tau}{k' g_0} a \Rightarrow \frac{da}{dN} = \frac{1}{k' g} a \quad (6)$$

in which $\Delta \sigma$ is applied stress range. τ , k' and g' are material parameters. By integrating from initial crack length a_i to final crack length a_f , the Eq. (6) can be deduced as

$$\int_{a_i}^{a_f} \frac{da}{a} = \int_{N_0}^{N_f} \frac{1}{k' g} dN \Rightarrow \Delta N \approx N_f - N_0 = k' g \ln \left(\frac{a_f}{a_i} \right) \quad (7)$$

Let γ denote the natural logarithm of the ratio of the final crack length to the initial crack length in Eq.(7), i.e.,

$$\gamma = \ln(a_f/a_i) \quad (8)$$

The initial crack length can be taken as the length of crack size [45], which also obeys the distribution in Eq. (2). While the final crack length is measured according to the fracture surface in Fig. 7, which is approximated to the half of semi-circumference for standard specimens, i.e., $a_f = \pi D_0/2$ (D_0 is diameter), and half of the diagonal for CHP specimens. Thus, the value and dispersion of γ for four different scales of CHP specimens are calculated in this work, as listed in Table 3.

3. Probabilistic life model considering the notch size effects

3.1. Weakest-link model in LCF regime

According to the basic idea of weakest-link method, the component can be regarded as a serial system composed of infinitesimal microcells when loaded, and thus the failure of any microcell may result in failure of the whole component. Suppose that the failure probability of each microcell unit V_0 is $p(V_0)$, then in general weakest-link theory model, the failure probability P_f of the component can be expressed as

$$P_f = 1 - \exp \left[- \int_V \ln[1 - p(V_0)] \frac{\partial N(V)}{\partial V} \delta V \right] \quad (9)$$

in which V is component volume and $N(V)$ is the number of microcracks within V . Assuming that the microcracks are evenly distributed and only one microcrack is in each microcell unit, i.e., $N(V) = V/V_0$. Then Eq. (9) can be derived as

$$P_f = 1 - \exp \left[- \int_V \ln[1 - p(V_0)] \frac{dV}{V_0} \right] \quad (10)$$

For brittle and quasi-brittle materials, the first principle stress law is utilized to determine whether the fatigue failure occurs in each microcell. Then, the failure probability of V_0 is

$$p(V_0) = p(V_0, \sigma_c > S_{-1}) \quad (11)$$

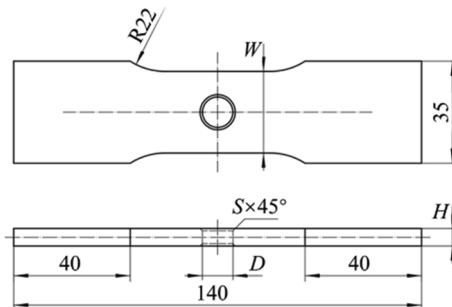


Fig. 1. Geometry of central hole plate specimen (unit in mm).

Table 1
CHP specimen with four different sizes.

Scale/%	D/mm	W/mm	H/mm	S/mm	K_t
100	10.5	28	6	0.8	2.321
80	8.4	22.4	4.8	0.6	2.336
60	6.3	16.8	3.6	0.5	2.353
40	4.2	11.2	2.4	0.3	2.357

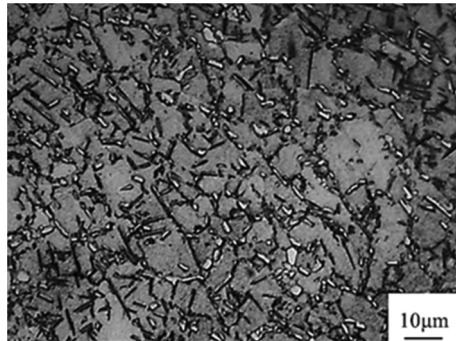


Fig. 2. Microstructural crystal phase of GH4169 superalloy.

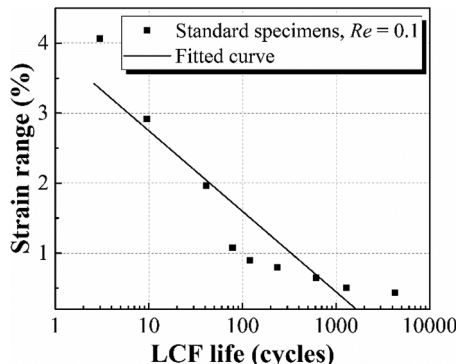
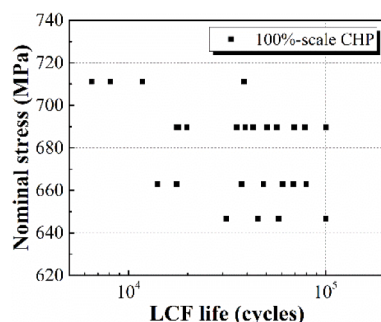


Fig. 3. LCF test results of standard specimens in GH4169 superalloy at 600 °C.

in which σ_e is the effective stress, S_{-1} represents the fatigue limit. The right side of the equation represents the failure probability of V_0 when σ_e is larger than S_{-1} . Griffith Law [46] is used to build the relationship between crack length and fatigue limit. By assuming the Weibull distribution of crack size, the fatigue limit also follows Weibull distribution. The weakest-link model based on Weibull function can then be obtained as



(a) 100 %-scale CHP specimen

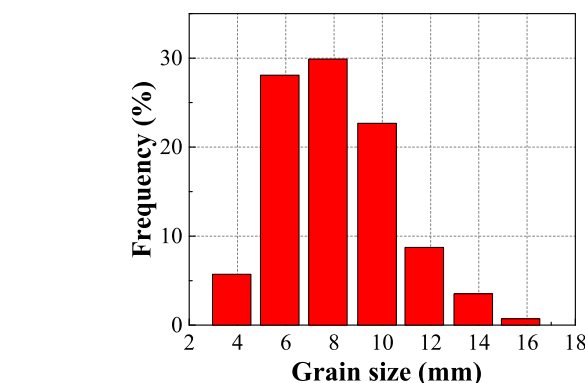


Fig. 5. Histogram of grain size for GH4169 superalloy.

Table 2
Material properties in fatigue life model of GH4169 superalloy.

Material	k	C	δw_0
Value	1.75	3.45e3	-1.97

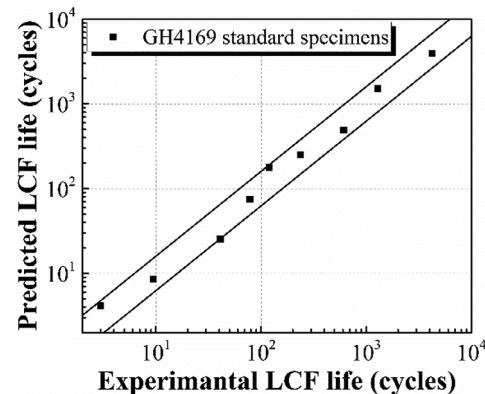
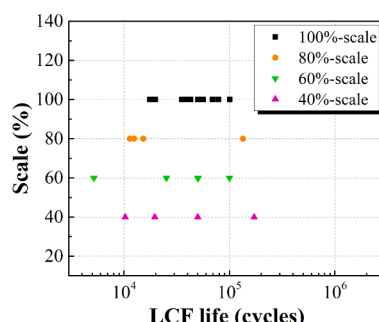


Fig. 6. Comparison between the experimental and predicted fatigue life.

$$P_f = 1 - \exp \left[- \int_V \left(\frac{\sigma}{\sigma_0} \right)^{b_\sigma} \frac{dV}{V_0} \right] \quad (12)$$

which is consistent with Eq. (1).

To sum up, there are three hypotheses used in the derivation of Weibull's weakest-link model for brittle and quasi-brittle materials: 1) A uniform spatial distribution of microcracks; 2) Weibull distribution of microcrack size; 3) Fatigue failure following the first principle stress law. For the LCF failure of ductile materials, hypotheses 1) and 2) can



(b) Four kinds of scale CHP specimens
(NS = 689.7 MPa)

Fig. 4. Test results for CHP specimens.

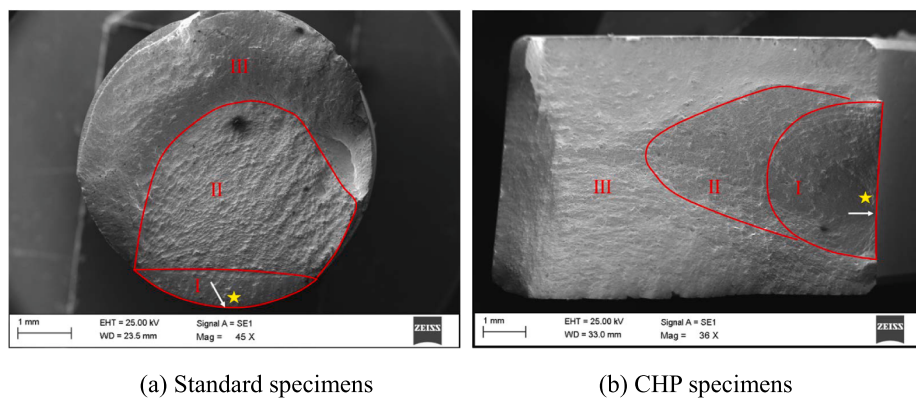


Fig. 7. Fracture surface morphology of GH4169 material in which I is the crack initiation zone, II is the crack propagation zone and III is the ductile fracture zone.

Table 3
Value and dispersion of γ for four scale specimens.

Scale		40%	60%	80%	100%
γ	Mean	1.74	2.78	3.86	6.63
	Std.	0.4677			
γ/γ (at 40%-scale)		1	1.60	2.21	2.89

be guaranteed, while hypothesis 3) is changed accordingly to use damage parameter to evaluate whether the component fails. Fatigue failure of V_0 will occur when the damage parameter w reaches the threshold value w_{th} , as

$$p(V_0) = p(V_0, w > w_{th}) \quad (13)$$

Considering the linear relationship between microcrack propagation rate and the damage parameter [47], a similar equation with Eq. (12) is obtained by conducting the same derivation process in Refs. [28,48,49], as

$$P_f = 1 - \exp \left[- \int_V \left(\frac{w}{w_0} \right)^m \frac{dV}{V_0} \right] \quad (14)$$

in which m is Weibull shape parameter, w_0 is normalized damage parameter. Since the elastic deformation of material is recoverable during the LCF process, the volume with plastic damage affects the fatigue life. Therefore, an effective volume V_E is introduced and the integration of Eq. (14) is performed in effective volume. Referred to the highly stressed volume [50], the effective volume is set as the volume with damage parameter greater than K times the maximum damage parameter w_{max} in the component, expressed as

$$V_E = \int_V [w > Kw_{max}] dV$$

$$[w > Kw_{max}] = \begin{cases} 1, & w > Kw_{max} \\ 0, & w \leq Kw_{max} \end{cases} \quad (15)$$

By substituting the effective volume in Eq. (15) into Eq. (14), Eq. (14) becomes

$$P_f = 1 - \exp \left[- \int_{V_E} \left(\frac{w}{w_0} \right)^m \frac{dV}{V_0} \right] \quad (16)$$

The hypotheses that need to be satisfied during the derivation of the weakest-link model based on damage parameter Eq. (16) are: (1) uniform distribution of microcracks, (2) Weibull distribution of microcrack size, and (3) damage parameter to determine fatigue failure.

In order to simplify Eq. (16), the effective damage parameter is introduced as

$$\bar{w} = \left(\frac{1}{V_0} \int_{V_E} w^m dV \right)^{1/m} \quad (17)$$

By substituting Eq. (17) into Eq. (16), the failure probability can then be expressed as the function of effective damage parameter as

$$P_f = 1 - \exp \left[- \left(\frac{\bar{w}}{w_0} \right)^m \right] \quad (18)$$

For uniformly stressed component, Eqs. (17) and (18) can be further simplified as

$$\bar{w} = \left(\frac{V}{V_0} \right)^{1/m} w \quad (19)$$

$$P_f = 1 - \exp \left[- \frac{V}{V_0} \left(\frac{w}{w_0} \right)^m \right] \quad (20)$$

As we can see from Eqs. (19) and (20), when the component is stressed uniformly, there is no geometric size effect. In this condition, parameter m characterizes the statistical size effect, and the effective damage parameter is determined by volume and damage parameter, as shown in Eq. (19). One the other hand, when the component is unevenly stressed, the effective damage parameter in Eq. (17) is the integral of damage parameter's function in the effective volume, characterizing both geometric and statistical size effects.

It can be obtained from Eq. (3) that for uniformly stressed specimen, the damage parameter $w_0(N_f)$ at a given fatigue life N_f can be approximated using Eq. (21), while at the effective damage parameter \bar{w} , the characteristic fatigue life N_0 can be estimated using Eq. (22).

$$w_0(N_f)^k \cdot N_f = C \quad (21)$$

$$\bar{w}^k \cdot N_0(\bar{w}) = C \quad (22)$$

By substituting Eqs. (21) and (22) into Eq. (18), the relationship between P_f and N_f can be obtained as

$$P_f = 1 - \exp \left[- \left(\frac{N_f}{N_0(\bar{w})} \right)^{b_N} \right] \quad (23)$$

$$b_N = \frac{m}{k} \quad (24)$$

in which b_N is Weibull shape parameter irrelevant to material volume, and N_0 is Weibull scale parameter dependent on the effective damage parameter. Substituting Eq. (22) into Eq. (23), the failure probability can be expressed as

$$P_f = 1 - \exp \left[- \left(\frac{N_f}{C/\bar{w}^k} \right)^{b_N} \right] \quad (25)$$

It is seen from Eq. (25) that the higher stress amplitude in the LCF process, the larger effective damage parameter, and so is the failure probability. For the specimens with volume V_1 and V_2 at the same failure probability, when the stress distribution at the gauge section is

the same, the relationship between the fatigue life and the volume can be deduced as

$$\frac{N_1}{N_2} = \left(\frac{\bar{w}_2}{\bar{w}_1} \right)^k = \left(\frac{V_{E2}}{V_{E1}} \right)^{1/b_N} = \left(\frac{V_2}{V_1} \right)^{1/b_N} \quad (26)$$

in which, N_1 and N_2 are fatigue lifetimes of V_{E1} and V_{E2} , respectively. Since the geometric size effect is the same for V_1 and V_2 , the ratio of the effective volume can be approximated to the ratio of the volume.

Combining Eq. (18) and Eq. (26), the relationship between the failure probability P_{f1} and P_{f2} under the same fatigue life can be expressed as

$$\frac{1}{V_1 \ln(1 - P_{f1})} = \frac{1}{V_2 \ln(1 - P_{f2})} \quad (27)$$

Furthermore, the failure probability for specimens with the volume V_1 can be utilized to predict the failure probability of volume V_2 , as

$$P_{f1} = 1 - [1 - P_{f2}]^{V_1/V_2} \quad (28)$$

Based on Eqs. (25) and (26), predicted failure probabilities for 60%, 80%, 100%-scale CHP specimens by using test data of 40%-scale are plotted in Fig. 8. Under the same failure probability, the test fatigue life is much longer than that by using weakest-link model, indicating that the weakest-link method cannot describe the statistical size effect well.

3.2. Calibrated weakest-link model during crack propagation

As is seen from Section 3.1, the size effect induced by the difference of microcracks in different volume is negative to fatigue life. However, the average fatigue life in different scales of CHP specimens in Fig. 4(b) is almost unchanged, as listed in Table 4. This phenomenon is consistent with the result of reduced activation ferrite/martenitic steels [51] and 30NiCrMoV12 [27] steel materials. It can be explained from the perspective of crack propagation, i.e., the critical crack length of is bigger for a larger volume specimen, thus the fatigue life is longer, especially for materials with a dominated crack propagation process. The combination of the negative and positive size effect results in a robust LCF fatigue behavior against the size effect.

Using Eq. (7) to explore the effect of crack propagation, the ratio of fatigue life for the specimens with different scales is defined as,

$$\frac{\Delta N_1}{\Delta N_2} = \frac{\ln(a_{f,1}/a_i)}{\ln(a_{f,2}/a_i)} \quad (29)$$

Based on Eq. (29), the distribution of failure probability for 60%, 80%, and 100%- scale CHP specimens can be shifted from the distribution of 40% scale CHP specimens by using weakest-link method, as shown in Fig. 9. After calibration of crack propagation, the predictions become closer to the test data. Then combining Eq. (26) and Eq. (29), the statistical size effect during the crack initiation and crack propagation can be superimposed by using the calibrated Weibull's weakest-link model, as

$$P_f = 1 - \exp \left[- \left(\frac{N_f}{\gamma N_0(\bar{w})} \right)^{b_N} \right] \quad (30)$$

Similarly, the Weibull's weakest-link model based on the effective damage parameter in Eq. (17) can be calibrated as

$$P_f = 1 - \exp \left[- \frac{1}{\gamma^{b_N}} \left(\frac{\bar{w}}{w_0} \right)^m \right] \quad (31)$$

4. Calibration of model parameters

4.1. Estimation of effective damage parameter

To estimate the fatigue life, stress and strain distributions of a component can be simulated by using FE method, and then post-processed to calculate \bar{w} . A simplified method is applied based on the assumption that the stress and strain in each element change linearly with the volume [14]. The effective damage parameter in Eq. (17) can be rewritten as the sum of each element's integral in the effective damage volume. By sorting the stress and strain amplitudes of the small volume for each FE from low to high, their distributions can be obtained. Using the volume of the i -th unit V_i , and the damage parameter w_i , Eq. (17) can be described as

$$\bar{w} = \left(\frac{1}{V_0} \sum_{i=1}^d \int_0^{V_i} [w_i(V)]^m dV \right)^{1/m} \quad (32)$$

The stress varies linearly between the minimum equivalent stress σ_i^{\min} and maximum equivalent stress σ_i^{\max} . So does the strain, as shown in Fig. 10, expressed as

$$\sigma_i(V) = \sigma_i^{\min} + (\sigma_i^{\max} - \sigma_i^{\min}) \frac{V}{V_i} \quad (33)$$

$$\varepsilon_i(V) = \varepsilon_i^{\min} + (\varepsilon_i^{\max} - \varepsilon_i^{\min}) \frac{V}{V_i} \quad (34)$$

in which subscript i represents the i -th element, and superscripts \min and \max denote the minimum and maximum values within an element, respectively.

By substituting Eqs. (33) and (34) into Eq. (35), the effective damage parameter can be calculated as

$$\begin{aligned} \bar{w} &= \left(\frac{1}{V_0} \sum_{i=1}^d V_i \bar{w}_i^m \right)^{1/m} = \left(\frac{1}{V_0} \sum_{i=1}^d V_i (\bar{w}_i - \delta w_0)^m \right)^{1/m} \\ &= \left(\frac{1}{V_0} \sum_{i=1}^d \frac{V_i}{m+1} \frac{(A_i - B_i - \delta w)^{m+1} - (B_i - \delta w)^{m+1}}{A_i - 2B_i} \right)^{1/m} \\ &\quad A_i = \Delta \varepsilon_{i,t}^{\min} \sigma_i^{\max} + \Delta \varepsilon_{i,t}^{\max} \sigma_i^{\min} \\ &\quad B_i = \Delta \varepsilon_{i,t}^{\min} \sigma_i^{\min} \end{aligned} \quad (35)$$

Eq. (35) is prone to numerical errors if denominator $(A_i - 2B_i)$ is small. Thus, when the value of $(A_i - 2B_i)$ is less than 0.01 MPa, the values of stress and strain in each element are assumed to be constant. To ensure the prediction accuracy, proper element size is important in FE analysis.

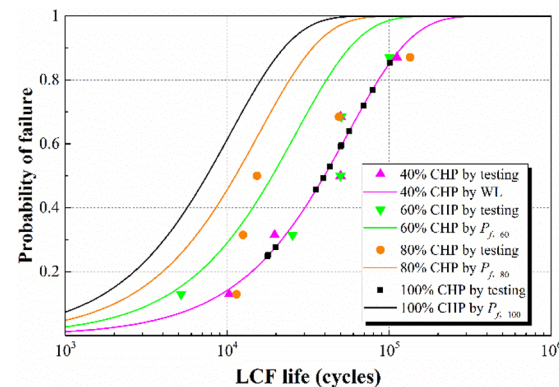
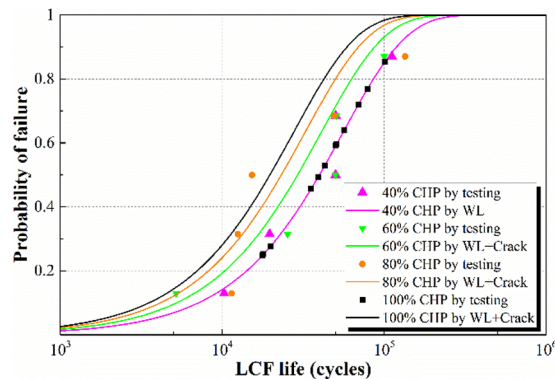
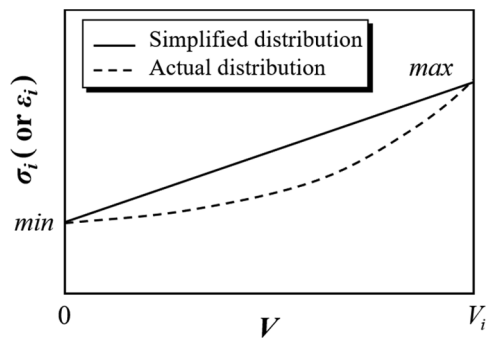


Fig. 8. Expected life considering the statistical size effect based only on weakest-link method.

Table 4

Average test fatigue life for specimens of four different sizes (NS = 689.7 MPa).

Scales	Numbers of specimens	Experimental mean life/cycles
100%	12	48,263
80%	4	44,585
60%	5	46,257
40%	5	48,338

**Fig. 9.** Expected life considering the statistical size effect based on weakest-link method and crack propagation calibration.**Fig. 10.** Comparison of linearly distributed stress/strain with actual distribution.

4.2. Bayesian calibration of Weibull shape parameter

In Eq. (30), b_N follows normal distribution and can be fitted by using multiple groups of test data [52]. After then, k can be calculated and used to determine effective damage parameter.

Since the failure probability is sensitive to the value of b_N , Bayesian calibration method is introduced to calibrate b_N to improve the prediction accuracy. Test results on CHP specimens are used for the calibration to obtain the posterior distribution of b_N . By setting the failure probability in Eq. (30) as 50%, the mean value of the number of cycles is estimated as

$$N_{f0} = \frac{N_0(\bar{w})(\ln 2)^{1/b_N}}{\gamma} \quad (36)$$

Take the logarithm of Eq. (36),

$$\ln N_{f0} = \ln N_0(\bar{w}) + \frac{1}{b_N} \ln 2 - \ln \gamma + \epsilon_r \quad (37)$$

in which ϵ_r is the fitting error and is assumed to follow Gaussian distribution with zero mean and a constant variance, i.e. $\epsilon_r \sim N(0, \sigma_\epsilon^2)$.

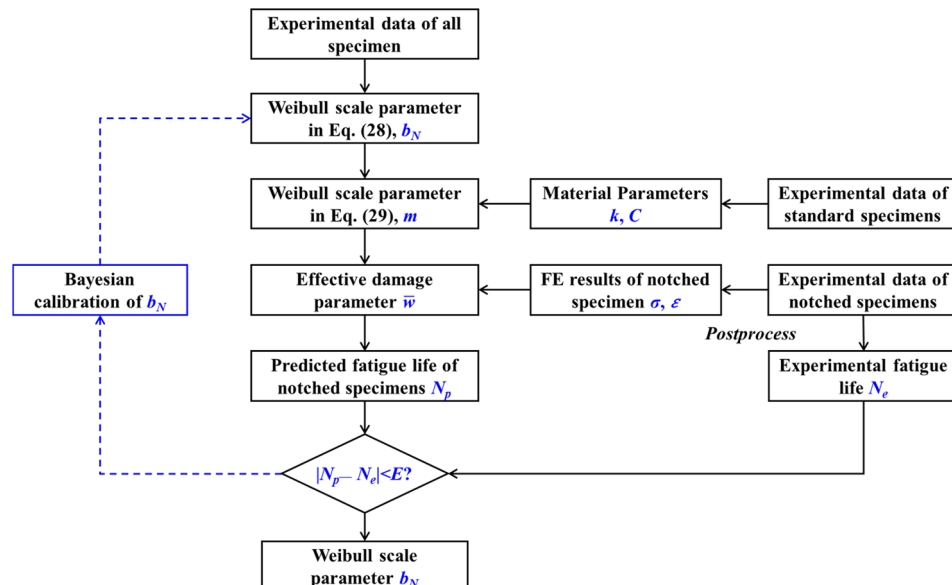
The likelihood distribution b_N , defined as the value under which the probability of specimen during the tests is the highest, follows

$$L(b_N) = f(N|b_N) \\ = \frac{1}{(2\pi)^{t/2}\sigma_\epsilon^t} \exp\left(-\frac{1}{2\sigma_\epsilon^2} \sum_{i=1}^t \left(\ln N_i - \left(\ln N_0(\bar{w}) + \frac{1}{b_N} \ln 2 - \ln \gamma\right)\right)^2\right) \quad (38)$$

in which t is the number of experimental results. The distribution of b_N by using statistical method in Eq. (38) is set as the prior distribution. Through multiplying the prior and likelihood distributions, the posterior distribution of b_N can be obtained as

$$P(b_N) = L(b_N|N) \propto \frac{1}{(2\pi)^{t/2}\sigma_\epsilon^t} \\ \exp\left(-\frac{1}{2\sigma_\epsilon^2} \sum_{i=1}^t \left(\ln N_i - \left(\ln N_0(\bar{w}) + \frac{1}{b_N} \ln 2 - \ln \gamma\right)\right)^2\right) \quad (39)$$

Markov Chain Monte Carlo (MCMC) method is then applied to calculate the posterior distribution by updating parameter, during which process the random walk Metropolis-Hastings algorithm [5] is

**Fig. 11.** Calibration framework for model parameters.

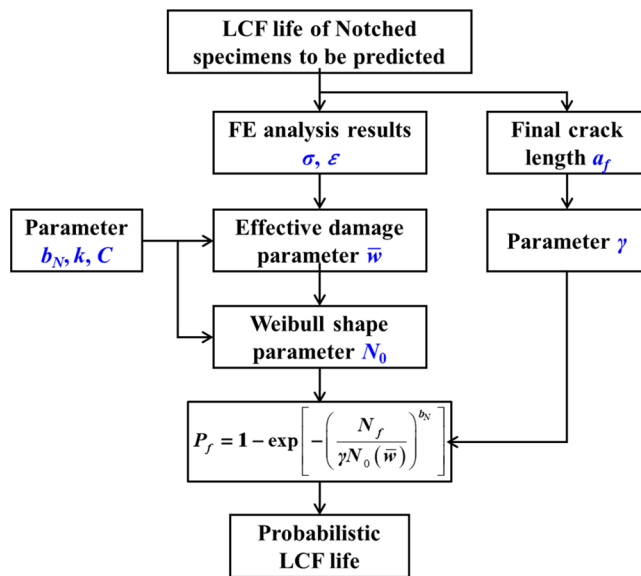


Fig. 12. Probabilistic fatigue life prediction considering the notch size effects.

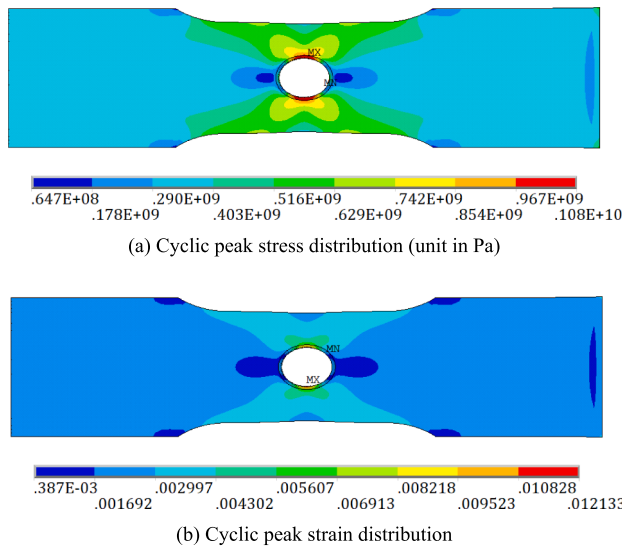


Fig. 13. FE results of GH4169 100%-scale CHP specimen ($NS = 711.2 \text{ MPa}$).

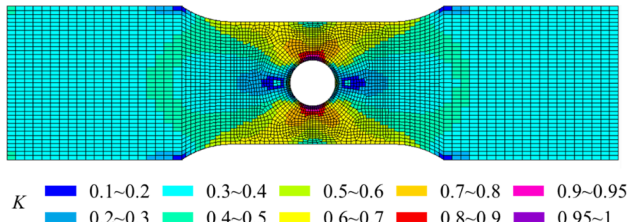


Fig. 14. Schematic diagram of effective damage volume for different ranges of K .

Table 5

Comparison of fatigue life for 100%-scale CHP specimens using different values of K .

K	0~0.9	0.9	0.95
Life dispersion error ΔN	4.0	4.2	4.5
Calculation time/s	7033	810	515

used to generate samples.

4.3. Iterated estimation of model parameters

Based on the above estimation process, the calibration framework for the model parameters is presented in Fig. 11, with detailed steps as:

Step 1: Estimating material parameter k , C and δw_0 by using test results on standard specimens based on Eqs. (3) and (4);

Step 2: Based on Eq. (30), the initial distribution of b_N is fitted using multiple groups of LCF test results;

Step 3: LCF tests on notched specimens are carried out to obtain the test fatigue lives. After then, FE analysis is conducted to obtain the effective damage parameter, which is used to predict the fatigue life and its distribution considering the notch size effects.

Step 4: Comparing the experimental and predicted average fatigue life for notched specimens. If the error is within the threshold, the distribution of b_N is obtained. Otherwise, b_N is updated by using Bayesian inference method and then repeat the calculation of predicted fatigue life in Step 3.

After obtaining the calibrated material parameters, the failure probability and then the probabilistic fatigue life can be calculated.

5. Probabilistic life prediction and discussion

5.1. Framework for the prediction of probabilistic fatigue life

After obtaining the model parameters, the probabilistic fatigue life can be predicted by employing the process shown in Fig. 12. The confidence band for the probabilistic fatigue life can be obtained considering the distribution of γ and b_N .

5.2. Initial distribution of b_N based on test results

Since the volume of component was uncorrelated with the shape parameter [52], both standard smooth specimens and CHP notched specimens were assumed to belong to a single population to compensate for the limited data sets. By sorting the life data from short to large under the same test condition, the failure probability of i -th specimen in total n specimens is calculated by using median rank estimation method [53], as

$$P_f(N_f) = \frac{i - 0.3}{n + 0.4} \quad (40)$$

Least square method is then used to fit Eq. (40) to calculate b_N under different loads, the results of which with the correlation coefficient larger than 0.9 are gathered to estimate the prior statistical distribution of b_N , as $b_N \sim N(1.30, 0.41^2)$.

5.3. Estimation of effective damage parameter

The FE analysis on 100%-scale CHP specimens under the actual test loading is simulated using commercial software ANSYS 15.0. The stress and strain distributions at the peak of cycle are shown in Fig. 13. The maximum stress and strain of GH4169 superalloy are 1080 MPa and 0.012, respectively.

Effective volume needs to be determined before calculating effective damage parameter. For CHP specimens, the range of effective volume corresponding to different values of K is shown in Fig. 14. The comparison of fatigue life for 100%-scale CHP specimens by using different values of K is listed in Table 5. As we can see, when K increases from 0 to 0.9, the effective damage parameter almost remains constant, so does the predicted fatigue life. When $K = 0.9$, the life dispersion error ΔN between the predicted life and the experimental data reaches 4.2. Furthermore, the life dispersion band increases to 4.5 when $K = 0.95$. It is shown that with the increase of K , the life dispersion error does not increase a lot, but the calculation time of post-processing fails

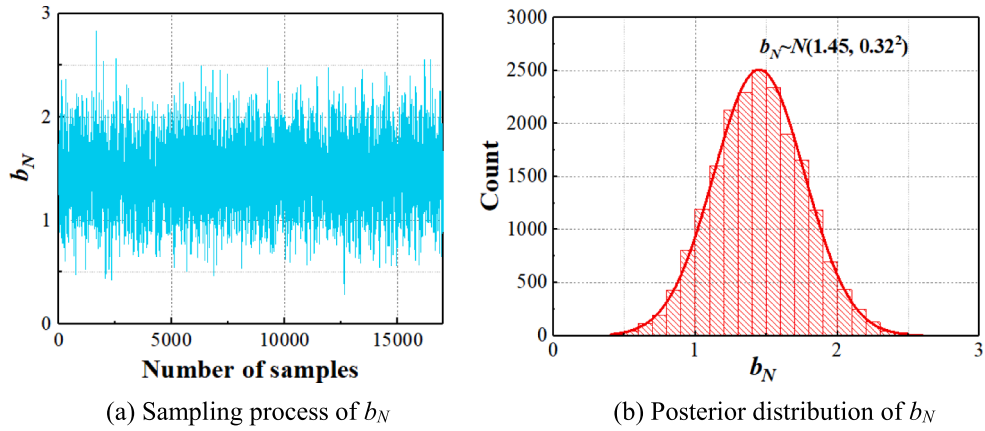


Fig. 15. Calibrated results for GH4169 superalloy.

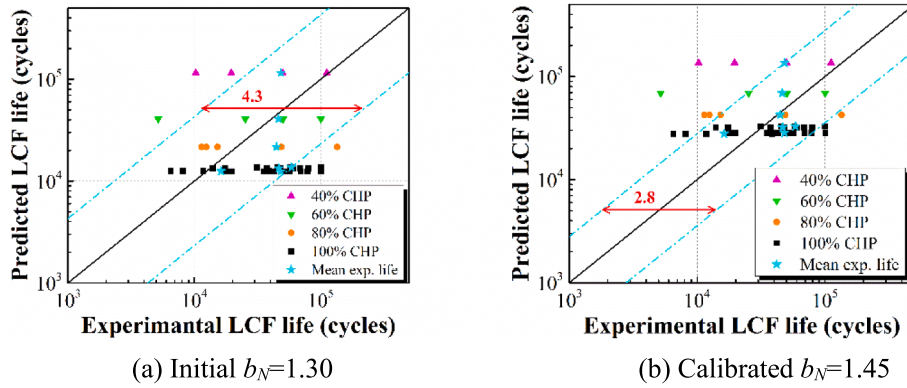


Fig. 16. Comparison of deterministic LCF life between experimental data and predicted results.

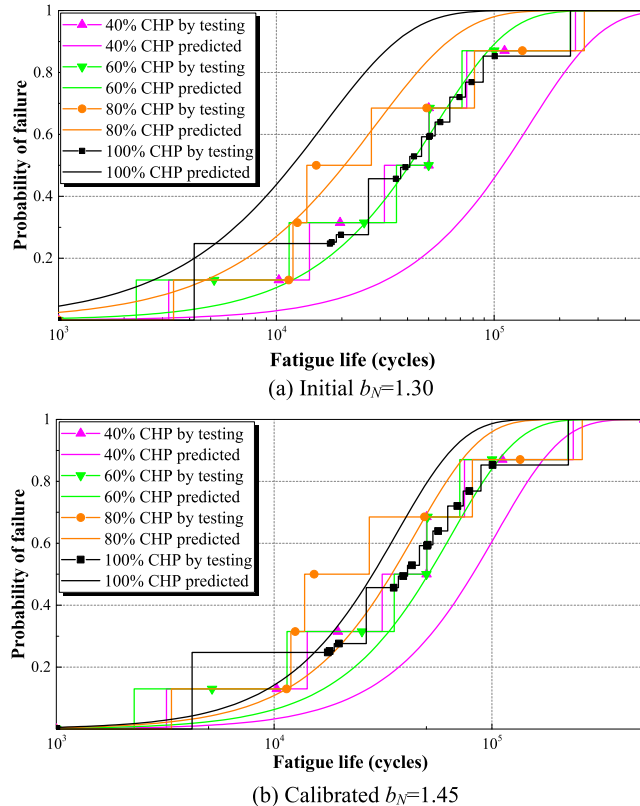


Fig. 17. Comparison of failure's probability between experimental data and predicted results.

significantly. Therefore, considering accuracy and efficiency, K is chosen as 0.9 in this study.

It is shown from Fig. 14 that large values of stress and strain concentrate at the upper/lower side of the hole when $K = 0.9$, meaning these regions belong to the effective volume. While the stress and strain are small at the left/right side away from the hole, thus for these regions the effect on LCF life is ignored at a larger K .

5.4. Calibration of b_N

Bayesian inference method is then applied to calibrate b_N based on the test data of 100%-scale CHP specimens. After the stable sampling process, posterior distribution of b_N are obtained, following $N(1.45, 0.32^2)$, as shown in Fig. 15. The mean value of b_N increases while the dispersion decreases after calibration.

After performing calibration, the mean value of b_N increases from 1.30 to 1.45, while the standard deviation decreases from 0.41 to 0.32. It is seen from Eq. (30) that the failure probability gets higher with the increase of b_N , i.e., predicted failure probability is conservative after calibrating b_N . Furthermore, the scatter of b_N becomes smaller due to supplementing the test data for calibration.

5.5. Probabilistic LCF life prediction and result analysis

The probabilistic LCF life model is finally obtained based on Eq. (31) as

$$P_f = 1 - \exp \left[-\frac{1}{\gamma} \left(\frac{N_f}{3.45 \times 10^3 \bar{W}^{1.75}} \right)^{1.45} \right] \quad (41)$$

By using the calibrated b_N , the deterministic LCF life for CHP specimens is predicted as shown in Fig. 16, in which the star symbols

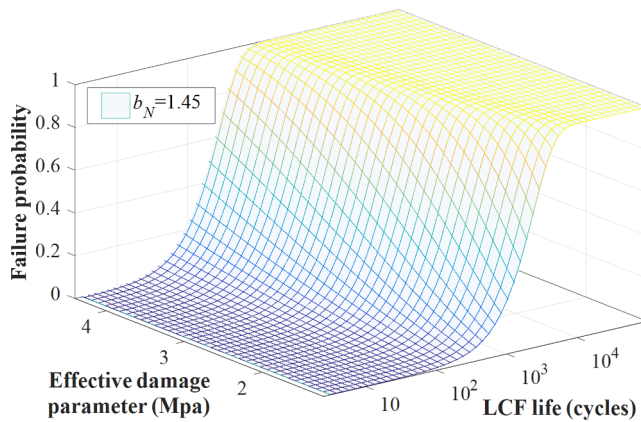


Fig. 18. Three-dimensional P_f - \bar{w} - N_f failure probability surface.

indicate the mean fatigue life. It is found that ΔN is reduced from 4.3 to 2.8, indicating that the accuracy of the deterministic LCF life prediction improves. It should be mentioned that the predicted error remains high for some CHP specimens due to the dispersion of the test data, especially for those with insufficient data, such as 40%- and 60%- scale specimens.

By comparing the predicted failure probability of CHP specimens at different scales when calibrating b_N , it is shown in Fig. 17 that the area enclosed by the predicted results and the test data is significantly reduced after calibration, meaning that the probabilistic results are significantly improved.

When b_N is taken as the mean value ($b_N = 1.45$ in this study), three-dimensional P_f - \bar{w} - N_f failure probability surface is obtained, as shown in Fig. 18. Based on P_f - \bar{w} - N_f surface, the LCF fatigue life for a certain component can be estimated by combining the test data for standard specimens with FE analysis of the component.

6. Conclusions

A calibrated weakest-link model based on damage parameter is established for probabilistic LCF life prediction of a component considering the notch size effects. The main contributions are summarized as follows:

- (1) The weakest-link model for a probabilistic life prediction is extended to LCF regime by introducing damage parameters. The derivation process as well as the necessary hypotheses is illustrated in this paper.
- (2) Experimental results show robustness of LCF resistance against specimen's size for CHP specimens because of the coexistence of negative size effect induced by the initial microcracks and positive size effect during the crack propagation. Considering the effect of crack propagation, a calibrated weakest-link model is established. The predicted results are in accordance with test data of CHP specimens with difference volumes.
- (3) To improve the accuracy of the proposed weakest-link model, a calibration process of Weibull parameters is established based on Bayesian inference method. After calibration, the error of average LCF life reduces from 4.3 to 2.8.
- (4) The weakest-link model can be used to estimate failure probability of LCF life for a notched component by combining the test results of standard specimens with effective damage parameter of the component.
- (5) This study enriches the probabilistic evaluation and design theory for the complicated mechanical components.

Declaration of Competing Interest

The authors declare that they have no known competing financial interests or personal relationships that could have appeared to influence the work reported in this paper.

Acknowledgements

We acknowledge financial support from the National Natural Science Foundation of China (Grant Nos. 51675024, 51305012 and 51375031), Civil Aircraft Major Project (MJ-2018-D-26) and National Science and Technology Major Project (2017-IV-0004-0041).

References

- [1] Makkonen M. Notch size effects in the fatigue limit of steel. *Int J Fatigue* 2003;25(1):17–26.
- [2] Kloos K. Einfluss des oberflächenzustandes und der probengröße auf die Schwingfestigkeitseigenschaften. *VDI-Berichte* 1976;268:63–76.
- [3] Taylor D. Geometrical effects in fatigue: a unifying theoretical model. *Int J Fatigue* 2000;21:413–20.
- [4] Araújo JA, Susmel L, Pires MST, et al. A multiaxial stress-based critical distance methodology to estimate fretting fatigue life. *Tribol Int* 2017;108:2–6.
- [5] Shlyannikov VN. Critical distance for creep crack growth problems. *Eng Fract Mech* 2017;176:126–43.
- [6] Santus C, Taylor D, Benedetti M. Determination of the fatigue critical distance according to the line and the point methods with rounded V-notched specimen. *Int J Fatigue* 2018;106:208–18.
- [7] Vargiu F, Sweeney D, Firrao D, et al. Implementation of the theory of critical distances using mesh control. *Theor Appl Fract Mech* 2017;92:113–21.
- [8] Fuentes JD, Cicero S, Procopio I. Some default values to estimate the critical distance and their effect on structural integrity assessments. *Theor Appl Fract Mech* 2017;90:204–12.
- [9] Taylor D. The theory of critical distances: a link to micromechanisms. *Theor Appl Fract Mech* 2017;90:228–33.
- [10] Lanning DB, Nicholas T, Palazotto A. HCF notch predictions based on weakest-link failure models. *Int J Fatigue* 2003;25(9–11):835–41.
- [11] Sadek S, Olsson M. The probability of HCF-Surface and sub-surface models. *Int J Fatigue* 2016;92:147–58.
- [12] Owolabi G, Okeyoyin O, Olasumboye A, et al. A new approach to estimating the fatigue notch factor of Ti-6Al-4V components. *Int J Fatigue* 2016;82:29–34.
- [13] Vale P, Härkegård G. A simplified method for weakest-link fatigue assessment based on finite element analysis. *Int J Fatigue* 2017;100:78–83.
- [14] Susmel L, Taylor D. The theory of critical distances to estimate lifetime of notched components subjected to variable amplitude uniaxial fatigue loading. *Int J Fatigue* 2011;33:900–11.
- [15] Susmel L, Taylor D. A critical distance/plane method to estimate finite life of notched components under variable amplitude uniaxial/multiaxial fatigue loading. *Int J Fatigue* 2012;38:7–24.
- [16] Yin T, Tyas A, Plekhov O, et al. A novel reformulation of the theory of critical distances to design notched metals against dynamic loading. *Mater Des* 2015;69:197–212.
- [17] Makkonen M. Statistical size effect in the fatigue limit of steel. *Int J Fatigue* 2001;23(5):395–402.
- [18] Wang R, Li D, Hu D, et al. A combined critical distance and highly-stressed-volume model to evaluate the statistical size effect of the stress concentrator on low cycle fatigue of TA19 plate. *Int J Fatigue* 2017;95:8–17.
- [19] Lei WS. A cumulative failure probability model for cleavage fracture in ferritic steels. *Mech Mater* 2016;93:184–98.
- [20] Weibull W. A statistical theory of the strength of materials. Generalstabens litografiska anstalts förlag; 1939.
- [21] Shirani M, Härkegård G. Fatigue life distribution and size effect in ductile cast iron for wind turbine components. *Eng Fail Anal* 2011;18(1):12–24.
- [22] Karolczuk A. Validation of the weakest link approach and the proposed Weibull based probability distribution of failure for fatigue design of steel welded joints. *Eng Fail Anal* 2016;67:46–62.
- [23] Wormsen A, Härkegård G. A statistical investigation of fatigue behaviour according to Weibull's weakest link theory. ECF15, Stockholm 2004; 2004.
- [24] Vu CC, Weiss J, Plé O, et al. Statistical size effects on compressive strength and mechanical behavior of concrete. *Key Eng Mater* 2017;754:317–20.
- [25] Ghannoum M, Baroth J, Rospars C, et al. Prediction of the size effect in concrete structures using an analytical approach to the weakest link and localization method (WL2). *Mater Struct* 2017;50(183):1–13.
- [26] Bazant ZP. Probability distribution of energetic-statistical size effect in quasibrittle fracture. *Probab Eng Mech* 2004;19(4):307–19.
- [27] Zhu SP, Foletti S, Beretta S. Evaluation of size effect on strain-controlled fatigue behavior of a quenched and tempered rotor steel: experimental and numerical study. *Mater Sci Eng, A* 2018;735:423–35.
- [28] Wormsen A, Sjödin B, Härkegård G, et al. Non-local stress approach for fatigue assessment based on weakest-link theory and statistics of extremes. *Fatigue Fract Eng Mater Struct* 2007;30(12):1214–27.

- [29] Li D, Hu D, Wang R, et al. A non-local approach for probabilistic assessment of LCF life based on optimized effective-damage-parameter. *Eng Fract Mech* 2018;199:188–200.
- [30] Makkonen L, Rabb R, Tikanmäki M. Size effect in fatigue based on the extreme value distribution of defects. *Mater Sci Eng, A* 2014;594:68–71.
- [31] Beretta S, Romano S. A comparison of fatigue strength sensitivity to defects for materials manufactured by AM or traditional processes. *Int J Fatigue* 2017;94:178–91.
- [32] Koyama M, Li H, Hamano Y, et al. Mechanical-probabilistic evaluation of size effect of fatigue life using data obtained from single smooth specimen: an example using Fe-30Mn-4Si-2Al seismic damper alloy. *Eng Fail Anal* 2017;72:34–47.
- [33] Murakami Y, Miller KJ. What is fatigue damage? A view point from the observation of low cycle fatigue process. *Int J Fatigue* 2005;27:991–1005.
- [34] Blasón S, Muniz-Calvente M, Koller R, et al. Probabilistic assessment of fatigue data from shape homologous but different scale specimens. Application to an experimental program. *Eng Fract Mech* 2017;185:193–209.
- [35] Zhu SP, Huang HZ, Smith R, et al. Bayesian framework for probabilistic low cycle fatigue life prediction and uncertainty modeling of aircraft turbine disk alloys. *Probab Eng Mech* 2013;34:114–22.
- [36] Kennedy MC, Ohagan A. Bayesian calibration of computer models. *J Roy Statist Soc: Ser B* 2001;63(3):425–64.
- [37] Wang R, Liu X, Hu D, et al. Zone-based reliability analysis on fatigue life of GH720Li turbine disk concerning uncertainty quantification. *Aerosp Sci Technol* 2017;70:300–9.
- [38] Ajami NK, Duan Q, Sorooshian S. An integrated hydrologic Bayesian multimodel combination framework: confronting input, parameter, and model structural uncertainty in hydrologic prediction. *Water Resour Res* 2007;43(1):208–14.
- [39] Shirazi CH. Data-informed calibration and aggregation of expert opinion in a Bayesian framework. University of Maryland, College Park; 2009.
- [40] Zhu S, Huang H, Peng W, et al. Probabilistic Physics of Failure-based framework for fatigue life prediction of aircraft gas turbine discs under uncertainty. *Reliab Eng Syst Saf* 2016;146:1–12.
- [41] Zhu S, Foletti S, Beretta S. Probabilistic framework for multiaxial LCF assessment under material variability. *Int J Fatigue* 2017;103:371–85.
- [42] ASTM Standard E606. Standard practice for strain-controlled fatigue testing. West Conshohocken, PA: ASTM International; 2012.
- [43] Smith KN. A stress-strain function for the fatigue of metals. *J Mater* 1970;5:767–78.
- [44] Tomkins B. Fatigue crack propagation-an analysis. *Phil Mag* 1968;18(155):1041–66.
- [45] Klotz T, Miao HY, Bianchetti C, et al. Analytical fatigue life prediction of shot peened Inconel 718. *Int J Fatigue* 2018;113:204–21.
- [46] Griffith AA, Gilman JJ. The phenomena of rupture and flow in solids. *Trans ASM* 1968;61:855–906.
- [47] Zuo JZ, Kermanidis AT, Pantelakis SG. Strain energy density prediction of fatigue crack growth from hole of aging aircraft structures. *Theor Appl Fract Mech* 2002;38(1):37–51.
- [48] Lei W. A generalized weakest-link model for size effect on strength of quasi-brittle materials. *J Mater Sci* 2018;53(2):1227–45.
- [49] Qian G, Lei WS. A statistical model of fatigue failure incorporating effects of specimen size and load amplitude on fatigue life. *Phil Mag* 2019;1–37.
- [50] Torrent R. A general relation between tensile strength and specimen geometry for concrete-like materials. *Matériaux et construction* 1977;10(4):187–96.
- [51] Hirose T, Sakasegawa H, Kohyama A, et al. Effect of specimen size on fatigue properties of reduced activation ferritic/martensitic steels. *J Nucl Mater* 2000;283:1018–22.
- [52] Wormsen A, Härkegård G. A statistical investigation of fatigue behaviour according to Weibull's weakest link theory. ECF15, Stockholm 2004; 2004.
- [53] Nelson WB. Accelerated testing: statistical models, test plans, and data analysis. John Wiley & Sons; 2009.